QUANTUM-BASED SPECTROSCOPY AND EFFICIENT ENERGY TRANSPORT WITH BIOMOLECULES

ROBERTO DE JESÚS LEÓN MONTIEL

under the supervision of
PROFESSOR JUAN P. TORRES

submitted this thesis in partial fulfillment
of the requirements for the degree of

Doctor

ICFO - INSTITUT DE CIÈNCIES FOTÒNIQUES
UNIVERSITAT POLITÈCNICA DE CATALUNYA

BARCELONA, 2014

Acknowledgements

The work presented in this manuscript represents four hard, yet exciting years of my life. It is important to say that nothing of what you are about to read would have been possible without the support of all the people I met during this journey.

First of all, I would like to thank my advisor Prof. Juan P. Torres for giving me the opportunity to work in his group. Looking for new research directions, Juan motivated me to work on the exciting field of Quantum Biology. Even though this field was new for both of us, thanks to Juan's advice and support, we achieved all the objectives we set ourselves at the beginning of my Ph.D.

I cannot imagine doing all this work without the support of my parents Sara Josefina Montiel Feria and Juan León de la Vega. Every day of my life, they have encouraged me to pursue my dreams without hesitation. *Muchas gracias por su apoyo ma y pa.* Also, I would like to thank my brother Juan León Montiel and my sister Miriam León Montiel for all the good advices that they have given to me.

It was an honor to work, discuss and socialize together with all of the Quantum Engineering of Light group: Adam Vallés, Carmelo Rosales Guzmán, Jiří Svozilík, and Luis José Salazar Serrano.

I would like to thank ICFO's Managment, Administration and Engineering departments. Thanks to them ICFO is an absolutely great place to work, where the only thing you need to worry about is your research project.

Finally, I want to thank all my friends. I will keep you guys in my heart forever. As you already know, I am terrible at remembering names so, to avoid forgetting someone, I just want to say thank you all. These years would not have been the same without you.

Abstract

For many years, the fields of quantum optics and biology have rarely shared a common path. In quantum optics, most of the concepts and techniques developed over the years stand for systems where only a few degrees of freedom are considered and, more importantly, where the systems under study are assumed to be completely isolated from their surrounding environment. This situation is far from what we can find in nature. Biological complexes are, by definition, warm, wet and noisy systems subjected to environmental fluctuations, where quantum phenomena are unlikely to be observed. Notwithstanding, in recent years, this paradigm has begun to be questioned by several works where quantum-mechanical concepts have been introduced in order to describe the dynamics of important biological processes, such as energy transport in photosynthetic light-harvesting complexes.

The goal of this thesis is twofold. Firstly, we will investigate how ideas and techniques routinely used in quantum optics can be exploited in order to develop new quantum-based spectroscopy techniques and, secondly, we will examine to what extent microscopic quantum phenomena could impact on the efficient transport behavior of photosynthetic light-harvesting complexes. This problem is particularly relevant, because the understanding of fundamental mechanisms that enable the highly efficient transport of energy in photosynthetic systems could lead us to the design of future quantum-inspired light-harvesting technologies, such as high-efficiency organic solar cells.

The present thesis is organized as follows. In chapter 1, we will present a new technique to enhance the robustness and sensitivity of an optical label-free imaging system based on the interaction of coherent resonant pulses with an arbitrary sample via stimulated Raman adiabatic passage (STIRAP), which is a phenomenon that benefits from quantum coherence in order to enhance the flow of energy between the two light beams involved in the stimulated Raman process. Using this technique, in combination with a high-frequency phase-sensitive detection scheme, we will demon-

strate that amazingly low concentration of atoms and molecules can be detected, up to 5 atoms of calcium and up to 20 molecules of neocyanine in a volume of 0.1 μm^3.

In chapter 2, we will use the light-matter interaction theory developed in the previous chapter to design a new experimental setup for measuring the temperature of atomic ensembles. The proposed scheme is based on a quantum interference effect that relates the temperature of an atomic ensemble with the emission cone width of Stokes photons that are spontaneously emitted when atoms are excited by an optical pulse. One of the attributes of this new technique is that, unlike commonly used time-of-flight measurements, the atomic cloud is not destroyed during each measurement.

The true role of entanglement in two-photon virtual-state spectroscopy, a two-photon absorption spectroscopy technique that allows one to retrieve information about the energy level structure of atoms or molecules, has been a controversial topic for years. In chapter 3, we will provide a thorough analysis of the virtual-state spectroscopy technique to show that, in the two-photon absorption process, the ability to obtain information about the energy level structure of a medium depends on the spectral shape of existing frequency correlations between the absorbed photons. Using this result, we will specify the type of two-photon source that is needed to experimentally implement virtual-state spectroscopy. In addition, by clarifying the role of entanglement in this technique, we will demonstrate that even paired photons carrying a low degree of entanglement, but with a proper spectral shape, can guarantee the successful retrieval of the energy level structure of the medium under study, thus showing that entanglement, by itself, is not the key ingredient to experimentally perform two-photon virtual state spectroscopy.

The last three chapters of this thesis are devoted to the description of energy transport in photosynthetic light-harvesting systems. In chapter 4, we will question recent claims that high-efficiency energy transport in light-harvesting complexes arises as a consequence of the quantum coherent evolution of the photosynthetic system and noise introduced by its surrounding environment, a process dubbed environment-assisted quantum transport or ENAQT. By using a classical stochastic model, we will explicitly demonstrate that highly efficient noise-assisted energy transport can be observed as well in purely classical systems. Using this result, we will propose an experimental setup, based on coupled classical electrical oscillators, where to observe the noise-assisted energy transport effect.

Motivated by the results presented in the previous chapter, we will implement, in chapter 5, the first phase of the experimental scheme proposed in chapter 4. It

consists of a setup that provides a unique tool to generate a tunable environment for classical electrical oscillators. We will illustrate the operation of the proposed setup by implementing the case of a damped random-frequency harmonic oscillator, where the tunability of the system is demonstrated by gradually changing the statistics of the oscillator's frequency distribution. The relevance of the proposed scheme resides in the fact that the high degree of tunability and control that it offers may allow us to design various types of noise with different probability distributions, which could be used in the study of non-Gaussian noise-induced effects. Moreover, it might allow us to study the transition from Markovian to non-Markovian dynamics of open systems.

In chapter 6, we provide the first study of the efficiency of photosynthetic energy transport where the initial excitation of the photosynthetic complex and the energy transfer to a reaction center are treated in more physically realistic ways. We will show that theoretical predictions are very sensitive to the details of these processes, especially to the energy transfer to the reaction center. We will demonstrate that the effect of ENAQT on the transport efficiency becomes negligible when considering more physically accurate models of energy transfer to a reaction center. Thus, we will call into question the widespread view that natural selection has optimized the interplay between quantum dynamics and noise in order to achieve a highly efficient photosynthetic energy transport.

Finally, because the topics addressed in this thesis are rather broad, we will present the conclusions in each chapter.

Resumen

Por muchos años, los campos de la óptica cuántica y la biología raramente han compartido un mismo camino. En la óptica cuántica, la mayoría de los conceptos y técnicas desarrolladas a lo largo de los años son válidas sólo en sistemas donde un número pequeño de grados de libertad es considerado y, más importante aún, donde se asume que los sistemas bajo estudio están completamente aislados del medio ambiente que los rodea. Esta situación está muy lejos de lo que podemos encontrar en la naturaleza. Los complejos biológicos son, por definición, sistemas a altas temperaturas, sujetos a fluctuaciones, en los cuales se cree que los fenómenos cuánticos son imposibles de observar. Sin embargo, en años recientes, esta creencia ha sido cuestionada por diferentes trabajos en los que conceptos de la mecánica cuántica han sido usados con el objetivo de describir la dinámica de procesos biológicos de gran importancia como, por ejemplo, el transporte de energía en los complejos de captación de luz en sistemas fotosintéticos.

El objetivo de esta tesis se divide en dos. Primeramente, investigaremos cómo las ideas y técnicas usadas comunmente en óptica cuántica pueden ser explotadas con el objetivo de desarrollar nuevas técnicas de espectroscopía y, segundo, estudiaremos hasta que punto los fenómenos cuánticos microscópicos pueden influir en el comportamiento del transporte eficiente de energía en sistemas fotosintéticos de captación de luz. Este problema es particularmente relevante, pues el entender los mecanismos fundamentales que permiten un eficiente transporte de energía en sistemas fotosintéticos nos podría conducir al diseño de nuevas tecnologías de captación y recolección de energía como, por ejemplo, celdas solares orgánicas de alta eficiencia.

La presente tesis está organizada de la siguiente forma. En el capítulo 1 presentaremos una nueva técnica para mejorar la robustez y sensibilidad de un sistema óptico de obtención de imágenes sin etiquetas, basado en la interacción de pulsos resonantes coherentes con una muestra biológica arbitraria a través del proceso conocido como paso adiabático estimulado de Raman o STIRAP por sus siglas en inglés, el cual hace

uso de la coherencia cuántica con el objetivo de mejorar el flujo de energía entre los dos haces de luz involucrados en el proceso estimulado de Raman. Usando esta técnica, en combinación con un esquema de detección de alta frecuencia, sensible a la fase, demostraremos que es posible detectar muy bajas concentraciones de átomos y moléculas; hasta 5 átomos de calcio y hasta 20 moléculas de neocyanine en un volumen de 0.1 μm^3.

En el capítulo 2, usaremos la teoría de interacción luz-materia desarrollada en el capítulo anterior, para diseñar un montaje experimental de medición de temperatura de ensambles atómicos. El esquema propuesto está basado en un efecto de interferencia cuántica que relaciona la temperatura de un ensamble atómico con el tamaño del cono de emisión de fotones Stokes, que son emitidos de forma espontánea cuando los átomos en el ensamble son excitados por un pulso óptico. Uno de los principales atributos de esta nueva técnica es que, a diferencia de los métodos de medición basados en el tiempo-de-vuelo de los átomos, TOF por sus siglas en inglés, la nube atómica no es destruída durante cada medición.

El verdadero papel que juega el entrelazamiento en la espectroscopía de estados virtuales, una técnica de espectroscopía de absorción de dos fotones que permite extraer información de la estructura energética de átomos y moléculas, ha sido un tema controversial por muchos años. En el capítulo 3, haremos un análisis exhaustivo de la técnica de espectroscopía de estados virtuales para mostrar que, en el proceso de absorción de dos fotones, la posibilidad de obtener información acerca de la estructura de los niveles de energía de un medio arbitrario, depende de la forma espectral de las correlaciones en frecuencia entre los fotones que son absorbidos por el medio. Usando este resultado, especificaremos el tipo de fuente de pares de fotones que es necesario para implementar experimentalmente la espectroscopía de estados virtuales. Adicionalmente, al clarificar el verdadero papel que juega el entrelazamiento en esta técnica, demostraremos que incluso pares de fotones débilmente entrelazados, pero con una forma espectral correcta, pueden garantizar la extracción exitosa de la estructura energética del medio bajo estudio, mostrando así, que el entrelazamiento por si sólo no es el ingrediente clave para realizar experimentalmente la espectroscopía de estados virtuales.

Los últimos tres capítulos de esta tesis están dedicados a describir el transporte de energía en sistemas fotosintéticos de captación de luz. En el capítulo 4, cuestionaremos recientes ideas en las que se describe a la alta eficiencia en el transporte de energía de complejos fotosintéticos como consecuencia de la interacción entre la evolución cuán-

tica del sistema y el ruido introducido por el medio ambiente que lo rodea, un proceso conocido como transporte cuántico asistido por ruido o ENAQT por sus siglas en inglés. Haciendo uso de un modelo clásico estocástico, demostraremos explícitamente que el transporte de energía de alta eficiencia asistido por ruido, puede ser observado también en sistemas puramente clásicos. Usando este resultado, propondremos un arreglo experimental, basado en osciladores electrónicos clásicos acoplados, donde se puede observar el efecto de transporte de energía asistido por ruido.

Motivados por los resultados presentados en el capítulo anterior, implementaremos, en el capítulo 5, la primera fase del esquema experimental propuesto en el capítulo 4. El esquema consiste en un montaje electrónico que permite generar ruido sintonizable para osciladores eléctricos clásicos. Mostraremos el funcionamiento del arreglo propuesto, implementando el caso de un oscilador armónico amortiguado con una frecuencia aleatoria. El control que ofrece nuestro sistema es demostrado al cambiar, de forma gradual, la estadística de la distribución de frecuencias del oscilador. La relevancia del sistema propuesto reside en que el alto nivel de control y sintonización que ofrece, puede ser utilizado para diseñar varios tipos de ruido con diferentes distribuciones de probabilidad que, a su vez, podrían ser utilizados en el estudio de efectos inducidos por ruido no-Gaussiano. Además, este arreglo experimental nos permitiría estudiar la transición de la dinámica Markoviana a no-Markoviana en sistemas abiertos.

En el capítulo 6, presentaremos el primer estudio de la eficiencia de transporte de energía fotosintética en el cual la excitación inicial del complejo fotosintético y la transferencia de energía al centro de reacción fotoquímico son tratados de una forma físicamente realista. Mostraremos que las predicciones teóricas son muy sensibles a los detalles de estos procesos, especialmente a la transferencia de energía al centro de reacción. Demostraremos que el efecto de ENAQT en la eficiencia de transporte es despreciable cuando se consideran modelos más precisos de transferencia de energía al centro de reacción. Usando este resultado, cuestionaremos la idea de que la selección natural ha optimizado la interacción entre la dinámica cuántica y el ruido, con el objetivo de alcanzar una alta eficiencia en el transporte fotosintético de energía.

Finalmente, debido a que los temas abordados en esta tesis son bastante amplios, presentaremos las conclusiones en cada capítulo.

List of publications

This thesis is based on the following publications:

- **R. de J. León-Montiel** and Juan P. Torres, *Enhancing the sensitivity and robustness of label-free imaging systems via stimulated Raman adiabatic passage*, New. J. Phys. **14**, 013018 (2012).
- **R. de J. León-Montiel** and Juan P. Torres, *Measurement of the temperature of atomic ensembles via which-way information*, Phys. Rev. A **85**, 033801 (2012).
- **R. de J. León-Montiel**, J. Svozilík, L. J. Salazar-Serrano, and Juan P. Torres, *Role of the spectral shape of quantum correlations in two-photon virtual-state spectroscopy*, New J. Phys. **15**, 053023 (2013).
- **R. de J. León-Montiel** and Juan P. Torres, *Highly efficient noise-assisted energy transport in classical oscillator systems*, Phys. Rev. Lett. **110**, 218101 (2013).
- **R. de J. León-Montiel**, J. Svozilík, and Juan P. Torres, *Generation of a tunable environment for electrical oscillator systems*, Phys. Rev. E **90**, 012108 (2014).
- **R. de J. León-Montiel**, Ivan Kassal, and Juan P. Torres, *The importance of excitation and trapping conditions in photosynthetic environment-assisted energy transport*, submitted.

Other publications by the author:

- S. Palacios, **R. de J. León-Montiel**, M. Hendrych, A. Valencia, and Juan P. Torres, *Flux enhancement of photons entangled in orbital angular momentum*, Opt. Express **15**, 14108 (2011).

List of publications

- J. Svozilík, **R. de J. León-Montiel**, and Juan P. Torres, *Implementation of a spatial two-dimensional quantum random walk with tunable decoherence*, Phys. Rev. A **86**, 052327 (2012).
- Y. A. de Icaza Astiz, V. G. Lucivero, **R. de J. León-Montiel**, and M. W. Mitchell, *Optimal signal recovery for pulsed balanced detection*, arXiv:1403.7085 [quant-ph].

Contents

Acknowledgements **v**

Abstract **vii**

List of publications **xv**

Contents **xvii**

1 Enhancing the sensitivity of label-free imaging systems via stimulated Raman adiabatic passage **1**

1.1 Basic equations 2

1.2 Robustness and high efficiency of STIRAP 4

1.3 Highly sensitive molecular detection 8

2 A new technique for measuring the temperature of atomic ensembles **11**

2.1 The model 12

2.2 Angular distribution of emitted Stokes photons 17

2.3 Experimental proposal 19

2.4 Heralded generation of the symmetric atomic state 20

3 Role of entanglement in two-photon virtual-state spectroscopy **23**

3.1 Light-matter interaction 25

3.2 TPA transition probability with uncorrelated classical pulses 28

3.3 TPA transition probability with classically correlated photons 29

3.4 TPA transition probability with entangled photons 30

3.4.1 Two-photon state with a Gaussian spectral shape 30

3.4.2 Two-photon state with a sine cardinal spectral shape 33

4 Highly efficient environment-assisted energy transport in classical oscillator systems 39

4.1 Quantum model 40
4.2 Classical model 41
4.3 Results: quantum vs classical 43

5 Generation of a tunable environment for electrical oscillator systems 47

5.1 The model 48
5.2 Experimental setup 49
5.3 Implementation and Results 51

6 Role of excitation and trapping conditions in photosynthetic energy transport 55

6.1 The model 56
6.1.1 Transfer to the RC 58
6.1.2 Initial excitation 59
6.2 Results 61
6.3 Discussion 63
6.3.1 Local transfer to the RC 63
6.3.2 FRET to the RC 64

Summary and Conclusions 67

Bibliography 69

A Appendix A 79

B Appendix B 81

C Appendix C 83

Chapter 1

Enhancing the sensitivity of label-free imaging systems via stimulated Raman adiabatic passage

Label-free optical imaging deals with the problem of detecting the presence of specific molecular species without the use of auxiliary alien substances, such as fluorophores. To address this issue, what is needed is an efficient, highly selective technique capable of sampling specific vibrations of atoms or molecules, and this can be provided by resonance Raman spectroscopy [1].

In 2008, an optical label-free imaging technique based on stimulated Raman scattering (SRS) was demonstrated [2, 3]. In this technique, the frequency difference between two pulses (pump and Stokes) is tuned in order to match the atomic frequency transition between two energy levels, which results in the depletion of the pump and, consequently, in the amplification of the Stokes beam via a stimulated Raman transition. Using a high-frequency phase-sensitive detection technique, Freudiger *et al.* [2] managed to measure a stimulated Raman loss (SRL) $\Delta E_p/E_p \sim 10^{-7}$, where E_p is the initial energy of the pump pulse and ΔE_p is the loss experienced by the pulse. This value of the SRL corresponds, for instance, to detecting a concentration of some 50μM (molecule number density of 10^{16} cm^{-3}) of retinol.

Here, we introduce a new technique that combines the above mentioned optical imaging scheme with a quantum optics technique that enhances the transfer of atomic populations, namely stimulated Raman adiabatic passage (STIRAP). Using a STIRAP

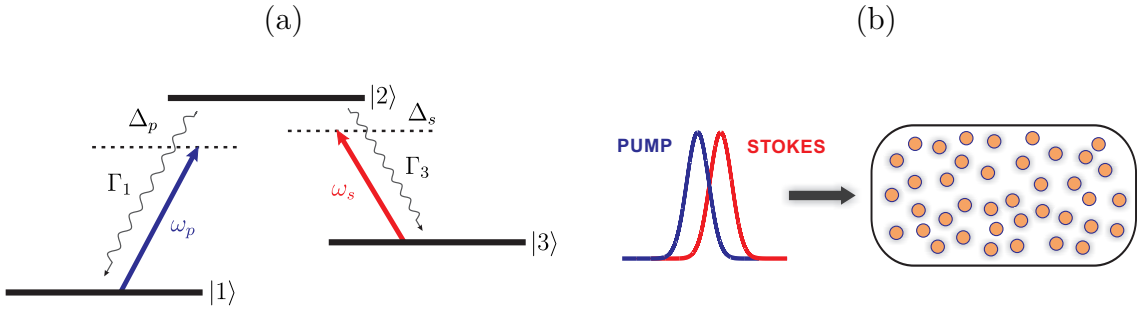

Fig. 1.1 (a) Scheme of a three-level system in Λ configuration. (b) Ensemble of three-level atoms shined by two temporally delayed classical pulses.

configuration, we show that one can, in principle, go beyond the current level of sensitivity, i.e., lowering the minimum concentration of molecules that can be detected, while at the same time enhancing the robustness of the system against variations in the laser parameters: intensities, detunings, pulse shapes, pulse widths and pulse delays. This high sensitivity could also be employed for detecting a larger number of molecules within a shorter acquisition time, which is of great importance in applications such as *in-vivo optical imaging*, a technique that requires primarily high speed.

This chapter is organized as follows. Section 2.1 provides the theoretical framework of the proposed technique. Section 2.2 describes the robustness and high efficiency that STIRAP can offer to label-free imaging systems. Finally, Section 2.3 shows how STIRAP could enable the detection of very low concentration of atoms and molecules.

1.1 Basic equations

Stimulated Raman adiabatic passage is a robust process that benefits from quantum coherence to enhance the population transfer between two quantum states of an atom, ion or molecule by means of two coherent light pulses [4–7]. In general, STIRAP can be modeled by considering an ensemble of atoms, with concentration N, where individual atoms are described as a three-level system in a Λ configuration, as depicted in Fig. 1.1. Each of the states is non-degenerate and there is no direct coupling between states $|1\rangle$ and $|3\rangle$. The atoms interact with two light pulses. The pump pulse, with central frequency ω_{p}, couples the state $|1\rangle$ with the intermediate state $|2\rangle$, and the Stokes pulse, with central frequency ω_{s}, couples the state $|3\rangle$ with the state $|2\rangle$. Because coherent phenomena are important in the STIRAP process, specific energy level configurations and nearly transform limited pulses are needed [8].

The Hamiltonian that describes the interaction of the atoms with the two pulses can be written in the rotating-wave approximation as [5]

$$H(t) = \frac{\hbar}{2}\begin{bmatrix} 0 & \Omega_{\mathrm{p}}^{*}(t) & 0 \\ \Omega_{\mathrm{p}}(t) & 2\Delta_{\mathrm{p}} & \Omega_{\mathrm{s}}(t) \\ 0 & \Omega_{\mathrm{s}}^{*}(t) & 2(\Delta_{\mathrm{p}} - \Delta_{\mathrm{s}}) \end{bmatrix}, \tag{1.1}$$

where $\Omega_{\mathrm{p}}(t) = -\boldsymbol{\mu}_{12} \cdot \mathbf{E}_{\mathrm{p}}/\hbar$ and $\Omega_{\mathrm{s}}(t) = -\boldsymbol{\mu}_{32} \cdot \mathbf{E}_{\mathrm{s}}/\hbar$ are the Rabi frequencies of the pump and Stokes pulses, respectively, and the coefficients $\boldsymbol{\mu}_{12}$ and $\boldsymbol{\mu}_{32}$ describe the dipole moments for each transition. Here, $\Delta_{\mathrm{p}} = \omega_{21} - \omega_{\mathrm{p}}$ and $\Delta_{\mathrm{s}} = \omega_{23} - \omega_{\mathrm{s}}$ correspond to the detunings of the pump and Stokes frequencies, respectively.

To introduce dissipation effects from level $|2\rangle$ to levels $|1\rangle$ and $|3\rangle$, we model the dynamics of the system by means of the Lindblad equation

$$i\hbar\frac{d\rho}{dt} = [H, \rho] + \mathcal{L}_{\mathrm{diss}}[\rho], \tag{1.2}$$

where ρ is the density matrix of the system and $\mathcal{L}_{\mathrm{diss}}$ is a Lindblad operator that describes the spontaneous emission within the three-level system. This operator is defined by [9]

$$\mathcal{L}_{\mathrm{diss}}[\rho] = \begin{bmatrix} -2\Gamma_1\rho_{22} & (\Gamma_1+\Gamma_3)\rho_{12} & 0 \\ (\Gamma_1+\Gamma_3)\rho_{21} & 2(\Gamma_1+\Gamma_3)\rho_{22} & (\Gamma_1+\Gamma_3)\rho_{23} \\ 0 & (\Gamma_1+\Gamma_3)\rho_{32} & -2\Gamma_3\rho_{22} \end{bmatrix}, \tag{1.3}$$

where Γ_1 and Γ_3 are the decay rates from state $|2\rangle$ to states $|1\rangle$ and $|3\rangle$, respectively.

The measurement of atom (molecule) concentrations in an extended area requires considering the changes of the pump and Stokes pulses while they propagate through the sample [10, 11]. If we make use of the slowly varying envelope approximation, the wave equations that describe the evolution of the pump and Stokes fields can be written, in terms of the corresponding Rabi frequencies, as [12]

$$\left(\frac{\partial}{\partial t} + \mathrm{c}\frac{\partial}{\partial z}\right)\Omega_{\mathrm{p}}(z,t) = -i\alpha_{\mathrm{p}}\rho_{12}^{*}, \tag{1.4}$$

$$\left(\frac{\partial}{\partial t} + \mathrm{c}\frac{\partial}{\partial z}\right)\Omega_{\mathrm{s}}(z,t) = -i\alpha_{\mathrm{s}}\rho_{32}^{*}, \tag{1.5}$$

where c is the speed of light and ρ_{ij} $(i,j = 1,2,3)$ are the elements of the density matrix

and ρ_{ij}^{*} stands for the complex conjugate of ρ_{ij}. The effect of the atomic medium on the pump and Stokes pulses propagation depends on the two absorption coefficients: $\alpha_{\mathrm{p}} = \omega_{\mathrm{p}} \mathrm{N} \left|\mu_{21}\right|^2 / \epsilon_0 \hbar$ and $\alpha_{\mathrm{s}} = \omega_{\mathrm{s}} \mathrm{N} \left|\mu_{23}\right|^2 / \epsilon_0 \hbar$, with ϵ_0 being the vacuum permittivity. In writing Eqs. (1.4) and (1.5) we have considered that the fields propagate parallel to the z-direction and that the medium is homogeneous, so atoms are assumed to be fixed and uniformly distributed within the ensemble. Equations (1.2), (1.4) and (1.5) constitute the mathematical description of the system under study. Due to the complexity of the system of partial differential equations, we need to numerically solve them in a moving frame defined by the variables $t' = t - z/\mathrm{c}$ and $z' = z$ (see Appendix A for further details).

1.2 Robustness and high efficiency of STIRAP

To provide a thorough analysis of the robustness and high efficiency that STIRAP can offer to label-free imaging systems, we have solved the set of equations described in the previous section by using a $^{40}\mathrm{Ca}^{+}$ ions ensemble as model system. In our simulations, we have considered the atomic levels $4^2S_{1/2}$, $4^2P_{1/2}$ and $3^2D_{3/2}$ for the states $|1\rangle, |2\rangle$ and $|3\rangle$, respectively. Their corresponding transition lifetimes are taken to be $\Gamma_1^{-1} = 7.7$ ns and $\Gamma_3^{-1} = 94.3$ ns. The initial condition of the atomic system is then defined by considering that atoms are initially in the state $|1\rangle$, so the elements of the initial density matrix read as

$$\rho_{11}(0) = 1, \quad \rho_{ij}(0) = 0 \quad (ij \neq 1). \tag{1.6}$$

For the light excitation, we assume that the initial pump and Stokes pulses exhibit a Gaussian shape given by

$$\Omega_{\mathrm{p,s}}(t) = \Omega_0 \exp\left\{-4 \ln 2 \left[(t \pm \tau/2)/\mathrm{T}\right]^2\right\}, \tag{1.7}$$

where T is the full pulse width at half maximum, Ω_0 is the peak Rabi frequency and τ is the temporal delay between the pulses. Notice that, in order to reduce harmful effects of the spontaneous decay, we need to employ light pulses with time duration much shorter than the lifetime of each transition.

To provide a point of comparison, in what follows, we will compare STIRAP with SRS based on overlapping pulses. Such comparison has been experimentally done for instance, in the picosecond multiphoton detection of sodium [13].

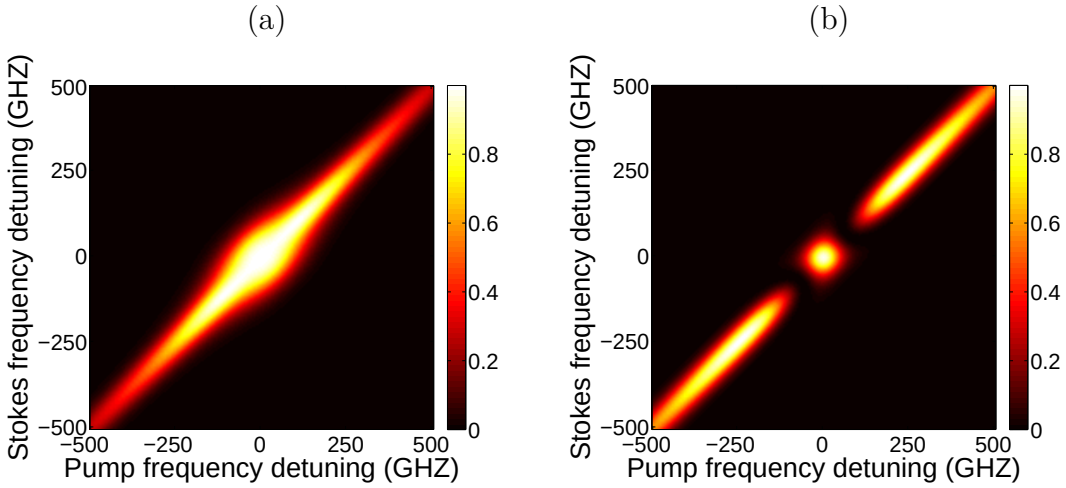

Fig. 1.2 Contour plot of the fraction of population transferred to level $|3\rangle$ as a function of the detuning from the atomic resonances of the pump (Δ_p) and the Stokes (Δ_s) pulses for (a) STIRAP, and (b) overlapping pulses.

STIRAP can achieve complete population transfer between states $|1\rangle$ and $|3\rangle$ if the quantum state of the atom can follow adiabatically one particular time-dependent eigenstate of the Hamiltonian given by Eq. (1.1), the so-called dark state [5]. Two conditions must be satisfied for trapping the system in a dark-state [4]. Firstly, the frequencies of the pulses need to be tuned to the two-photon resonance regime, i.e., $\Delta_p = \Delta_s$. Figure 1.2 shows the fraction of population transferred to the state $|3\rangle$ as a function of the detunings of the pump and Stokes pulses. Notice from Fig. 1.2(a) that one-photon resonance ($\Delta_p = \Delta_s = 0$) is not a requisite for achieving an efficient transfer of population when using a STIRAP configuration. In contrast, when performing SRS with overlapping pulses, the amount of atomic population transferred to the state $|3\rangle$ do in fact depend on the one-photon condition, as shown in Fig. 1.2(b).

The second and most distinguishing condition is that the evolution of the fields must be adiabatic, following a counterintuitive ordering of the light pulses [14]. The system starts with all the population in the ground state $|1\rangle$ and the Stokes field Ω_s is applied first. In this case, the initial state of the system corresponds exactly to the dark state. Afterwards, Ω_p is adiabatically increased and, at the same time, Ω_s is decreased until the condition $\Omega_p \gg \Omega_s$ is reached. In this scenario, all the population can be transferred to the state $|3\rangle$, with almost 100% efficiency.

We can produce nearly complete population transfer between states $|1\rangle$ and $|3\rangle$ when the pump and Stokes pulses overlap. However, SRS with overlapping pulses

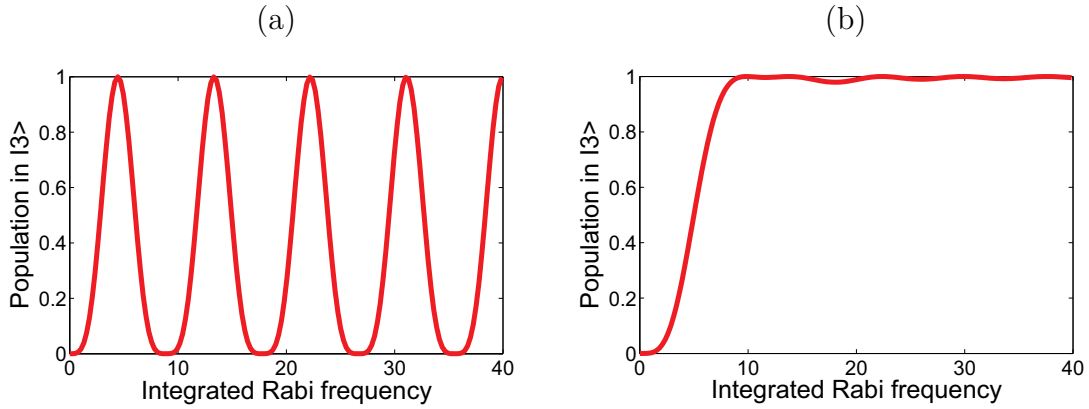

Fig. 1.3 Fraction of atomic population transferred to level $|3\rangle$ as a function of the integrated Rabi frequency of pulses with time duration T = 10 ps and pulse delays (a) $\tau = 0$, (b) $\tau = 0.55$ T.

is not so robust against changes in the shape or intensity of the pulses, features that could change due to variations in the laser parameters or the propagation of the pulses through the ensembles. Figure 1.3 shows the fraction of atoms that reach state $|3\rangle$ as a function of the integrated Rabi frequency, i.e. $A = \int \Omega(t)\, dt$, for the case of overlapping pulses ($\tau = 0$) and the STIRAP configuration with temporal delay $\tau = 0.55$T. To understand why STIRAP is more robust against changes in the pulse shapes than the overlapping pulses configuration, let us assume that the initial pulses have an initial Rabi frequency Ω_0 so that $A = 13$, which corresponds to nearly 100% population transfer in both configurations. For the case of overlapping pulses, increases of 10% in the integrated Rabi frequency of the pulses diminish the population transfer to $\sim 50\%$, while decreases of 10% produce a population transfer of $\sim 70\%$. On the contrary, in the STIRAP regime, a nearly complete transfer of population is produced within the same range of variations.

Information about the number of atoms or molecules that constitute the sample under study is retrieved by measuring the stimulated Raman Gain (SRG), i.e. $\Delta E_s/E_s$, where ΔE_s is the gain in energy of the Stokes pulse and E_s is the energy carried by the initial Stokes pulse. As previously mentioned, the integrated Rabi frequency is set to $A = 13$, which maximizes the transfer of population for both the SRS with overlapping and non-overlapping pulses, as depicted in Fig. 1.4(a).

Figure 1.4(b) shows the change of SRG as a function of the distance traversed by the pulses through a sample with an ion number density of 10^{18} cm^{-3}. We can observe that the SRG is always higher in the STIRAP configuration. Furthermore,

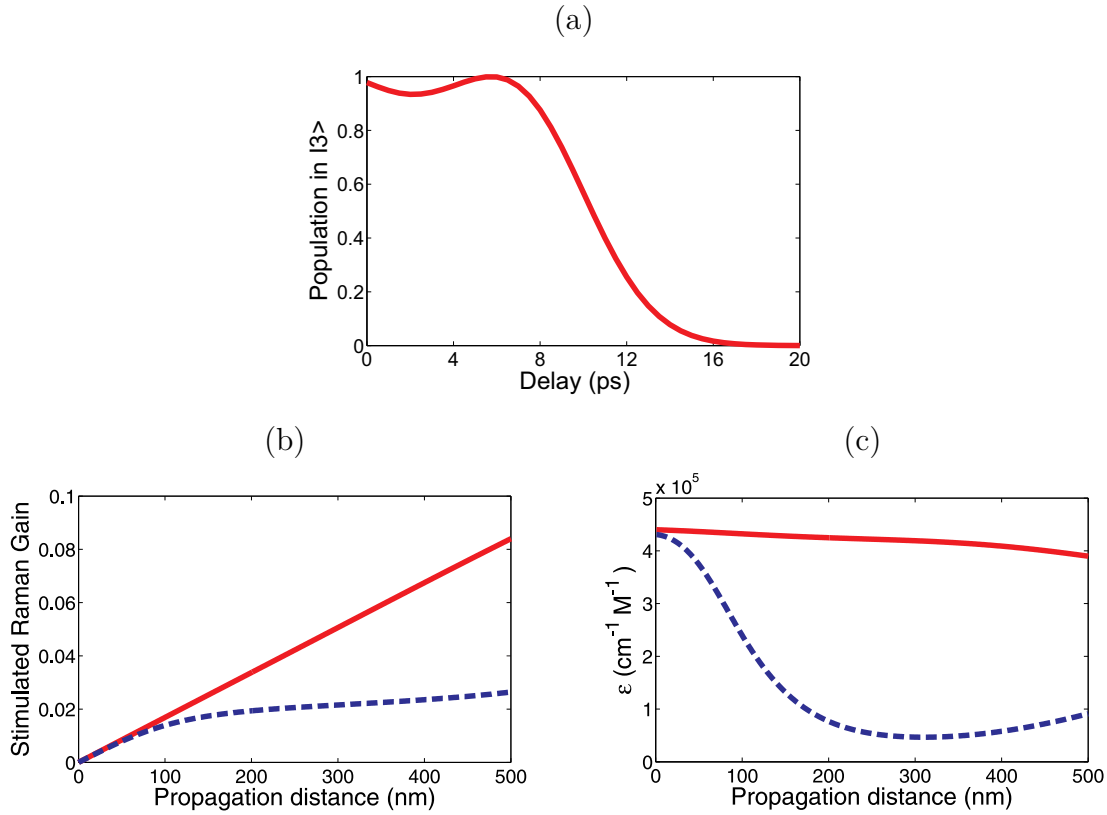

Fig. 1.4 (a) Population transferred to level $|3\rangle$ as a function of the delay between pulses. (b) SRG as a function of the propagation distance through a sample with an ion number density of 10^{18} cm^{-3}. (c) Molar amplification coefficient as a function of the distance. Solid line: STIRAP; dashed line: overlapping pulses.

the information provided by Fig. 1.4(b) can be used in order to analyze how the light absorption changes when propagating along the sample. To this end, we compute the effective molar amplification coefficient ϵ, which is a measure of how strongly a sample absorbs light at a given wavelength. This coefficient is defined by $\epsilon = A/\mathrm{N}L$, where A is the absorbance of the sample and L is the pathlength [15]. Figure 1.4(c) shows the effective molar amplification (in units of $\mathrm{M}^{-1}\mathrm{cm}^{-1}$) as a function of the propagation distance. Notice that, in the initial stages of propagation, the pulses experience small changes that do not affect the absorption properties of the sample. However, as the pulses continue to propagate, their shapes and temporal delays start to change [see Fig. 1.5(a)]. One can see that, even though the changes in the integrated Rabi frequency are comparable in both cases [see Fig. 1.5(b)], the effective molar amplification coefficient remains practically unchanged for STIRAP, while it decreases in the case of overlapping pulses.

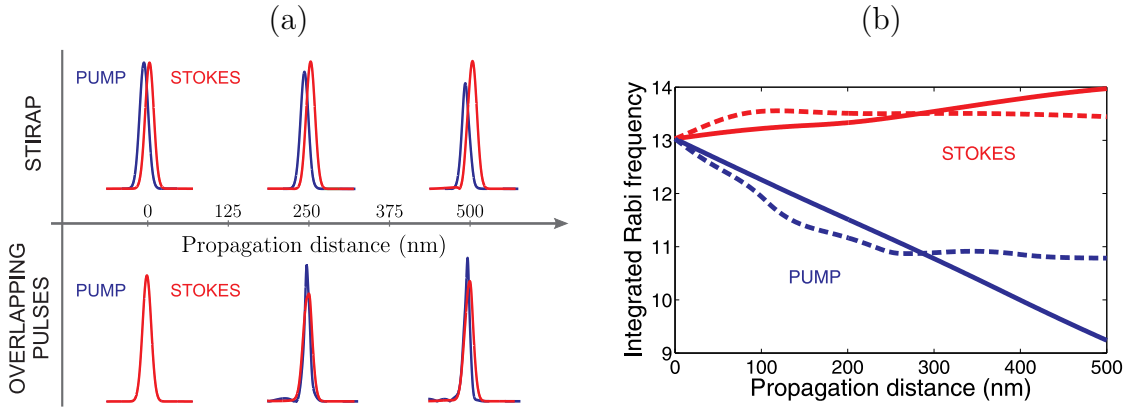

Fig. 1.5 (a) Shapes of the pump and Stokes pulses during propagation. (b) Evolution of the integrated Rabi frequency of the pulses propagating in STIRAP (solid line) and overlapping pulse (dashed line) configurations.

We have observed that when considering samples containing a high concentration of atoms or molecules ($> 10^{18}$ cm^{-3}), the SRG is always higher with STIRAP. However, as we will see in the next section, for low concentration samples, variations in the SRG are no longer due to propagation through the sample, but to the precise preparation of the initial pulses.

1.3 Highly sensitive molecular detection

Optical imaging based on SRS is especially suited for detecting very low concentrations of atoms or molecules. In particular, the combination of such technique together with STIRAP provides a higher sensitivity than the commonly used overlapping pulses configuration.

Figure 1.6 shows that in low concentration samples, both SRS configurations yield the same linear dependence between concentration and SRG, with an effective molar amplification coefficient $\epsilon = 440000$ M^{-1}cm^{-1}. This value of the molar amplification coefficient represents a sensitivity enhancement that would allow us to detect concentrations of up to $\sim 10^{13}$ cm^{-3}. We can observe from Fig. 1.6(b) that SRS with STIRAP always achieves a higher sensitivity than SRS with overlapping pulses. Moreover, notice that fractional changes in the initial integrated Rabi frequency do not modify substantially the molar amplification coefficient in the case of STIRAP; whereas in the case of overlapping pulses, a fractional change of 20% could severely affect the sensitivity.

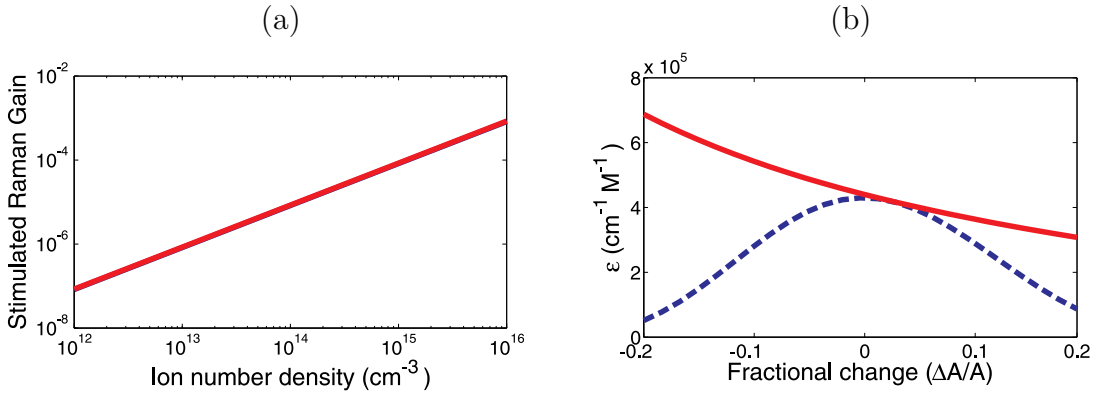

Fig. 1.6 (a) Stimulated Raman Gain as a function of the ion number density. (b) Molar amplification coefficient as a function of the fractional change in the integrated Rabi frequency of the pulses initially prepared in STIRAP (solid line) and overlapping pulse (dashed line) configurations. Propagation distance is set to $L = 500$ nm.

At this point, we have presented the efficiency enhancement for detecting Calcium ions; however, since our interest resides in molecular systems, we now turn our attention to ensembles of neocyanine molecules. This molecule is of great chemical interest due to its intense absorption (180000 $\mathrm{M}^{-1}\mathrm{cm}^{-1}$) and short excited lifetimes ($\sim$ 120 ps) [16]. Because of these properties, neocyanine has already been considered as a test molecule in experimental realizations of label-free imaging [17, 18].

The level configuration for neocyanine is shown in Fig. 1.7(a). Transitions $|1\rangle \rightarrow |2\rangle$ and $|3\rangle \rightarrow |2\rangle$ are excited by laser pulses with central wavelength of 770 nm and 850 nm, respectively. We illuminate the sample with 15 fs pulses and a time delay of 9.33 fs between them (STIRAP configuration). The laser is set to have 4 mW average power and 80 MHz repetition rate. For the sake of comparison with Refs. [17, 18], we have assumed that the pulses have a transversal section S$\sim$ 1 $\mu\mathrm{m}^2$ and that they propagate 100 nm within the sample. From these parameters, we obtain a volume in the laser focus of 10^{-19} m^3 (10^{-16} L).

Figure 1.7(b) shows the SRG as a function of the neocyanine concentration. Notice that by using a STIRAP configuration we can obtain an effective molar amplification coefficient of $\epsilon = 11350$ $\mathrm{M}^{-1}\mathrm{cm}^{-1}$. This value of the molar amplification coefficient represents a sensitivity enhancement that would allow us to detect concentrations of up to ~ 0.5 μM, which is a concentration ten and two times smaller than previously reported in Refs. [17] and [18], respectively.

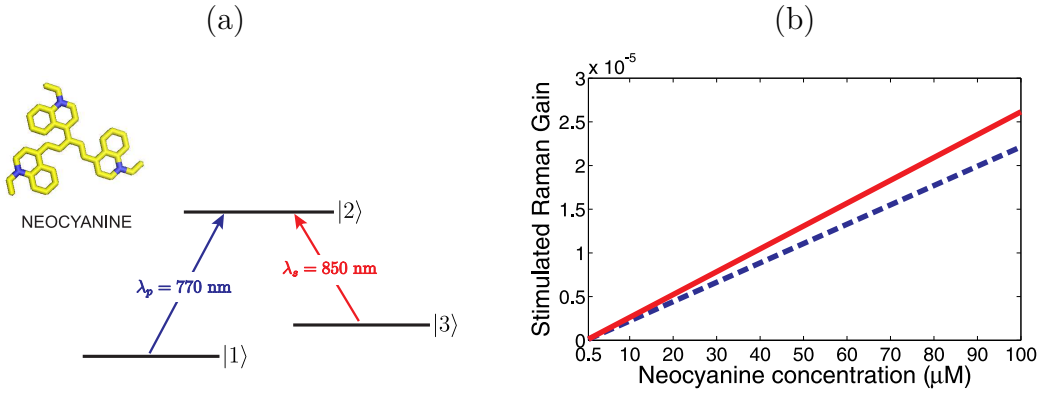

Fig. 1.7 (a) Scheme of the neocyanine three-level configuration. (b) Stimulated Raman Gain as a function of the concentration of neocyanine for pulses propagating in STIRAP (solid line) and overlapping pulse (dashed line) configurations. Propagation distance is set to $L = 100$ nm. The figure of neocyanine molecule was drawn using PyMOL [19].

Conclusions

In this chapter, we have described a new technique to enhance the robustness and sensitivity of an optical label-free imaging technique based on SRS. The proposed technique is based on the interaction of coherent resonant pulses with a specific sample via stimulated Raman adiabatic passage. In principle, in combination with a high-frequency phase-sensitive detection scheme, it allows one to detect amazingly low concentrations of atoms and molecules. For instance, with an effective molar amplification coefficient of 440000 $\mathrm{M}^{-1}\mathrm{cm}^{-1}$ and SRG $> 10^{-7}$, it is possible to detect $n \sim 10^{-7}S/(2.303\epsilon)$ ions, which for $S \sim 10\ \mu\mathrm{m}^2$ yields $n \sim 5$ ions.

In the case of molecular ensembles, we have shown that using a STIRAP configuration, an effective molar amplification coefficient of 11350 $\mathrm{M}^{-1}\mathrm{cm}^{-1}$ can be obtained. For this value of the molar coefficient, a SRG $> 10^{-7}$ and $S \sim 1\ \mu\mathrm{m}^2$, we could experimentally detect $n \sim 20$ neocyanine molecules, which is two times smaller than the lowest reported value.

We have observed that when using a STIRAP configuration, the SRG remains linear with respect to the concentration of molecules and the propagation distance traveled by the pulses, which enables a straightforward quantitative analysis. Finally, we have demonstrated that STIRAP is less sensitive to changes in the energy or shape of the initial pulses, which would make it easy to experimentally carry out under realistic experimental conditions.

Chapter 2

A new technique for measuring the temperature of atomic ensembles

Atomic ensembles provide a robust platform for many theoretical and experimental schemes for the implementation of several quantum information protocols [20, 21] and, in particular, for the generation of paired photons with non-classical correlations [22, 23]. In these photon-generation schemes, a weak classical field (pump pulse) interacts with an atomic ensemble leading to the spontaneous emission of a photon with a lower energy (Stokes photon). Since the Stokes photon and the atomic ensemble are highly correlated, the projection of the Stokes photon results in the generation of an atomic state that is a coherent superposition of all possible states of the ensemble where only one atom is excited, the so-called collective atomic state [24].

Although in most experiments the emitted Stokes photons are detected at small angles ($\sim 0^\circ - 3^\circ$) [22, 23, 25–27], the direction in which they can be emitted from the atomic cloud has been a subject of study for years. For instance, it has been shown that in the case of room-temperature ensembles, where atoms are considered to move fast within the cloud, Stokes photons are emitted within a small cone around the direction of propagation of the pump beam [28, 29]. In contrast, for the case in which atoms are considered to be fixed in their positions, as in cold atomic ensembles, Stokes photons have no preferred direction of emission [30, 31], always that it is not forbidden by the transition matrix elements. These results consider only the angular distribution of emitted photons in two limiting cases: when atoms are either moving very fast (high temperature) or completely fixed (low temperature) within the cloud.

However, the transition between these two cases had not been investigated before.

In this chapter, we construct a theoretical model that allows us to describe the angular distribution of emitted Stokes photons as a function of the temperature of the atomic ensemble. Then, by making use of this model, we develop a new technique where the measurement of the width of the Stokes emission cone is used to determine the temperature of the atomic cloud. Moreover, we demonstrate that such measurement can be done thanks to the close relationship that exists between the range of possible directions of emission, and the *which-way* information available about where the photon originated, i.e., knowledge of the position of the atom that emitted the photon during the light-matter interaction. The importance of the proposed technique resides in the fact that, unlike commonly used time-of-flight measurement [32], the atomic cloud is not destroyed during each measurement. Therefore, this new technique takes a place in the group of nondestructive measurements, such as resonance fluorescence spectrum analysis [33], recoil-induced resonances [34], and transient four-wave mixing [35], with the difference that it does not require any additional elements in the basic writing-reading experimental setup, which makes it appealing for its implementation.

This chapter is organized as follows. Section 2.1 presents the developed theoretical model. In Section 2.2, we make use of the new model to investigate the angular distribution of emitted Stokes photons as a function of the temperature of the atomic ensemble. Finally, Section 2.3 describes the proposed experimental scheme for measuring the temperature of atomic clouds.

2.1 The model

Imagine the scenario where an ensemble of N identical three-level atoms in Λ configuration (Fig. 2.1) is illuminated by a weak laser pulse coupling the transition $|g\rangle \rightarrow |e\rangle$ with a detuning Δ. Then, after some time, spontaneous decay of an atom in the ensemble leads to the generation of a photon with different wavelength (Stokes photon), leaving the atom in the symmetric state $|s\rangle$. In this situation, how could we know the direction in which the Stokes photon is emitted? Furthermore, how would the path of the photon be related, if so, to the temperature of the ensemble? To address these questions, we proceed as follows.

We consider the pump beam as a slowly varying classical field propagating along the z direction, with a Rayleigh range much larger than the length of the atomic

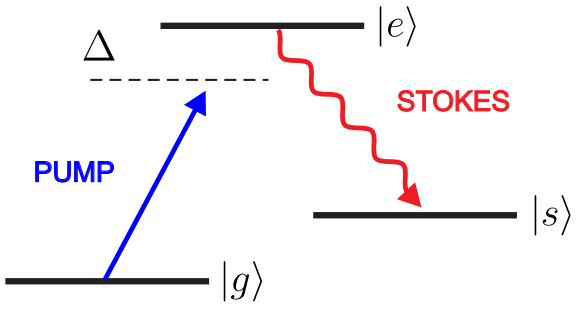

Fig. 2.1 Three-level atom in Λ configuration. Transition from the ground $|g\rangle$ to the excited state $|e\rangle$ is produced by a weak pump pulse with detuning Δ. After excitation, a photon with lower energy (Stokes photon) is spontaneously emitted, leaving the atom in the symmetric state $|s\rangle$.

ensemble, defined as

$$E_{\mathrm{p}}\left(\mathbf{r},t\right)=u\left(\mathbf{r}_{\perp}\right)\xi(t)\exp\left\{ik_{0}z-i\omega_{0}t\right\}+\mathrm{H.c.},\tag{2.1}$$

where $\omega_0 = k_0 \mathrm{c}$ is the central frequency, c is the speed of light, $u\left(\mathbf{r}_{\perp}\right)$ describes the transverse spatial shape of the pump beam and $\xi(t)$ its temporal shape. Here, H.c. stands for the Hermitian conjugate.

Because only one Stokes photon is emitted by the ensemble, the Stokes field is taken as a quantum field described by the expression

$$\hat{E}_{\mathrm{s}}^{\dagger}\left(\mathbf{r},t\right)=\int\hat{a}(\mathbf{k})\exp\left\{i\mathbf{k}\cdot\mathbf{r}-i\omega t\right\}d\mathbf{k},\tag{2.2}$$

where $\hat{a}(\mathbf{k})$ is the annihilation operator, $\mathbf{k}=(k_x,k_y,k_z)$ is the wavevector of the Stokes photon and $\omega = |\mathbf{k}|\mathrm{c}$ its frequency.

To model the interaction of the light fields with the atomic ensemble, we make use of the Hamiltonian [28]

$$H(t)=\sum_{i=1}^{N}\hat{\sigma}_{sg}^{i}\int d\mathbf{k}g_{\mathbf{k}}a^{\dagger}(\mathbf{k})\exp\left\{i\Delta\omega t\right\}u\left(\mathbf{r}_{\perp,i}\right)\xi\left(t\right)\exp\left\{-i\Delta\mathbf{k}\cdot\mathbf{r}_{i}\right\}+\mathrm{H.c.},\tag{2.3}$$

where $\hat{\sigma}_{sg}^{i}=|s\rangle_{i}\langle g|$ is the transition operator for the ith atom, $\mathbf{r}_i=(x_i,y_i,z_i)$ is the vector position of the ith atom, $g_{\mathbf{k}}$ is the coupling coefficient of the transition, $\Delta\omega=\omega-(\omega_0-\omega_{sg})$ and $\Delta\mathbf{k}=\mathbf{k}-k_0\hat{z}$, with ω_{sg} being the transition frequency between states $|g\rangle$ and $|s\rangle$.

For the initial conditions of the system, we assume that, before the interaction, all

the atoms are in the ground state and that there are no Stokes photons in the optical modes, so the initial state of the system reads

$$|\Psi\rangle_0 = |g_1...g_i...g_N\rangle \otimes |0\rangle_{\mathbf{k}}\,. \tag{2.4}$$

Then, considering that the pump field is weak enough, we can make use of first-order perturbation theory to write the state of the system as

$$|\Psi\rangle = |\Psi\rangle_0 - i\,\varepsilon\,(\Delta\omega)\sum_{i=1}^{N}\int d\mathbf{k}\; u\,(\mathbf{r}_{\perp,i})\exp\{-i\Delta\mathbf{k}\cdot\mathbf{r}_i\}\,|g_1...s_i...g_N\rangle\,|\mathbf{k}\rangle, \tag{2.5}$$

where $\varepsilon(\Delta\omega) = \int_0^t dt' g\,\xi(t')\exp(i\Delta\omega t')$. In writing Eq. (2.5), we have assumed that $\Delta\mathbf{k}$ is independent of the frequency, $|\mathbf{k}| \simeq k_0$, and that the coupling is the same for all allowed directions of emission of the Stokes photons, $g_{\mathbf{k}} = g$.

Before we continue with the description of the model, it is important to remark that the use of first-order perturbation theory is motivated by the experiments in which a weak pump pulse and a short interaction time are used in order to guarantee that the probability of creating more than one excitation in the collective atomic state is very low [23, 25–27]. Therefore, the weak-pumping condition makes a perturbative approach suitable for describing a realistic situation.

Making use of Eq. (2.5), we can recover the cases presented in Refs. [28–31], namely the emission of Stokes photons from *cold* and *hot* atomic ensembles. In the former case, since the atoms are considered to be fixed in their positions, we can directly use Eq. (2.5) to find that the probability of emitting a photon in a given direction $\mathbf{k}$ is the same for all directions (i.e., there is no preferred direction of emission) independently of the specific shape of the atomic cloud. In contrast, in the latter case, due to the fact that during the light-matter interaction the atoms are moving fast, an average over all positions $\mathbf{r}_i$ should be performed [28, 36], so the state of the systems takes the form

$$|\Psi\rangle = |\Psi\rangle_0 - i\varepsilon\,(\Delta\omega)\int d\mathbf{k}\; F\,(\Delta\mathbf{k})\,|\mathbf{k}\rangle \otimes \sum_{i=1}^{N}|g_1...s_i...g_N\rangle\,, \tag{2.6}$$

where the average value over all positions is defined as

$$F\,(\Delta\mathbf{k}) = \int d\mathbf{r} u(\mathbf{r}_\perp)\exp\{-i\Delta\mathbf{k}\cdot\mathbf{r}\}\,\mathrm{P}_{\mathrm{dis}}(\mathbf{r}), \tag{2.7}$$

with $\mathrm{P}_{\mathrm{dis}}(\mathbf{r})$ being the atomic distribution function. Using Eq. (2.6), one can obtain that the Stokes photons are emitted in a small cone around the direction of the pump

(see Refs. [28, 29] for a detailed calculation), whose width depends on the particular spatial shape of the atomic cloud. Notice that, in this case, the photon and atomic degrees of freedom can be decoupled, and the quantum state of the atoms corresponds to the so-called symmetric collective atomic state, i.e., $|s_a\rangle = 1/\sqrt{N}\ \sum_1^N |g_1...s_i...g_N\rangle$.

Notice that the transition from the two limiting cases, cold and hot atomic ensembles, cannot be explored by means of Eq. (2.5), because it does not show any temperature dependence. However, we can model this dependence by introducing a new function describing the movement of each atom as a function of the ensemble's temperature. This new function writes

$$f(\mathbf{r}, \mathbf{r}_i) = \frac{1}{\pi^{3/2} A^3(T)} \exp\left[-\frac{|\mathbf{r} - \mathbf{r}_i|^2}{A^2(T)}\right], \tag{2.8}$$

where $\mathbf{r}_i$ is the mean position of the ith atom and the function $A(T) = \mathrm{v}_a \tau$ determines the radius of the area over which the atoms can move during the interaction time. It depends on the pump pulse duration τ, and on the speed ($\mathrm{v_a} = \sqrt{2K_B T/m}$) most likely to be possessed by any atom of the system. m is the mass of the atom, K_B is the Boltzmann constant and T is the temperature of the atomic ensemble. Notice that the origin of $\mathrm{v_a}$ lies in the Maxwell−Boltzmann distribution. This distribution is assumed, because it has been shown that the Maxwell-Boltzmann distribution provides an accurate description of the motion of atoms at temperatures above tenths of μK [32, 37]. Therefore, Eq. (2.8) is useful for describing the motion of atoms undergoing a transition from the hot to the cold condition, provided that the lowest temperature values are above tenths of μK.

By substituting Eq. (2.8) into Eq. (2.5), we find that the temperature-dependent quantum state of the system atoms-photon can be written as

$$\begin{aligned} |\Psi\rangle = |\Psi\rangle_0 - i\varepsilon(\Delta\omega) \sum_{i=1}^{N} \int d\mathbf{k} \int_V d\mathbf{r} f(\mathbf{r}, \mathbf{r}_i)\, u(\mathbf{r}_\perp) \\ \times \exp\{-i\Delta\mathbf{k} \cdot \mathbf{r}\} |g_1...s_i...g_N\rangle |\mathbf{k}\rangle, \end{aligned} \tag{2.9}$$

where V stands for the volume of the cloud. Notice that, in the limit where $A \to 0$ (cold atomic ensemble), the function given in Eq. (2.8) tends to a Dirac delta function, and we recover the state of the system described by Eq. (2.5).

To obtain the angular distribution of the emitted Stokes photons, we trace out the atomic variables of the density matrix of the system, i.e., $\rho = |\Psi\rangle \langle\Psi|$. Neglecting the

vacuum contribution, the reduced density matrix of the photon state writes

$$\rho_{\mathrm{s}} = \sum_{i=1}^{N} \int d\mathbf{k} d\mathbf{k}' S(\mathbf{r}_i, \mathbf{k}) S^*(\mathbf{r}_i, \mathbf{k}') |\mathbf{k}\rangle\langle\mathbf{k}'|, \tag{2.10}$$

where

$$S(\mathbf{r}_i, \mathbf{k}) = \int_V d\mathbf{r} f(\mathbf{r}, \mathbf{r}_i) u(\mathbf{r}_\perp) \exp\left(-i\Delta\mathbf{k}\cdot\mathbf{r}\right). \tag{2.11}$$

Considering that the atoms are contained in a cell with transversal dimensions L_x, L_y and length L_z, we can solve Eq. (2.11) to obtain

$$S(\mathbf{r}_i, \mathbf{k}) = \frac{1}{8}\alpha^2 \Phi(x_i, k_x)\Phi(y_i, k_y)\Omega(z_i, k_z), \tag{2.12}$$

where

$$\alpha = \left(\frac{r_0^2}{A^2 + r_0^2}\right)^{1/2}, \tag{2.13}$$

$$\begin{aligned}\Phi(x_i, k_x) = &\exp\left[-\frac{k_x^2 r_0^2}{4} - \left[\frac{\alpha}{r_0}\left(x_i + i\frac{r_0^2 k_x}{2}\right)\right]^2\right] \\ &\times \left\{\mathrm{erf}\left[-\frac{\alpha^3}{2}\left(2x_i - ik_x A^2 - \frac{L_x}{\alpha^2}\right)\right]\right. \\ &\left. - \mathrm{erf}\left[-\frac{\alpha^3}{2}\left(2x_i - ik_x A^2 + \frac{L_x}{\alpha^2}\right)\right]\right\},\end{aligned} \tag{2.14}$$

$$\begin{aligned}\Omega(z_i, k_z) = &\exp\left[-\frac{k_z^2 A^2}{4} - ik_z z_j\right] \\ &\times \left\{\mathrm{erf}\left[-\frac{1}{2A}\left(2z_i - ik_z A^2 - L_z\right)\right]\right. \\ &\left. - \mathrm{erf}\left[-\frac{1}{2A}\left(2z_i - ik_z A^2 + L_z\right)\right]\right\}.\end{aligned} \tag{2.15}$$

Notice that the presence of the error function [erf(x)] in Eqs. (2.14) and (2.15) is due to the integration over the finite volume V of the cell that contains the atoms.

Finally, we can find that the probability of emitting a Stokes photon in the direction $\mathbf{k}$ is given by the diagonal terms of the density matrix (2.10),

$$P(\mathbf{k}) = \sum_{i=1}^{N} \left|S\left(\mathbf{r}_i, \mathbf{k}\right)\right|^2, \tag{2.16}$$

where the normalization condition writes $\sum_{i=1}^{N} \int d\mathbf{k} \left|S\left(\mathbf{r}_i, \mathbf{k}\right)\right|^2 = 1$. In general, because

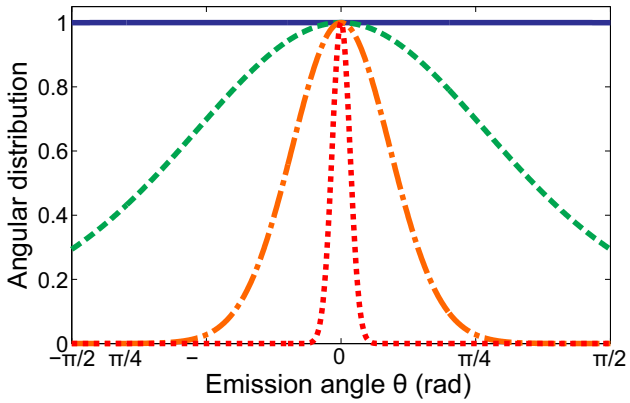

Fig. 2.2 Angular distribution of emitted Stokes photons for different temperatures of the atomic ensemble. Solid line: $T = 100$ μK; Dashed line: $T = 1$ K; Dash-dotted line: $T = 10$ K; Dotted line: $T = 300$ K. In all cases, the pump pulse duration is set to $\tau = 10$ ns.

the atomic cloud contains a large atom number density, the atomic summation can be rewritten as $\sum_{i=1}^{N} \to (N/V) \int dV$.

Notice that, in order to obtain the angular distribution of photons as a function of the temperature, equation (2.16) needs to be solved numerically due to the presence of the error function in Eqs. (2.14) and (2.15). However, since the functions of the spatial variables are separated [as can be seen from Eq. (2.12)], the numerical integration can be easily performed.

2.2 Angular distribution of emitted Stokes photons

We have computed the angular distribution of the emitted Stokes photons considering an ensemble of ^{87}Rb atoms contained in a pencil-shaped cell with transversal dimensions: $L_x = L_y = 2$ mm, and length $L_z = 30$ mm. The atoms are illuminated by a pump pulse with a transversal shape given by $u(\mathbf{r}_\perp) \sim \exp\{-(x^2 + y^2)/r_0^2\}$, where $r_0 = 2$ mm is the beam waist of the pump beam. The level configuration of the atoms is set to $5^2P_{1/2}$ for the excited level $|e\rangle$, and the Zeeman-splitting levels $5^2S_{1/2}\,(F = 1)$ and $5^2S_{1/2}\,(F = 2)$ for the $|g\rangle$ and $|s\rangle$ states, respectively.

Figure 2.2 shows the angular distribution (normalized to the maximum) of emitted Stokes photons as a function of the angle θ between the direction of the pump and the emitted photon [as shown in Fig. 2.3(a)]. In the low temperature limit, the

spontaneous emission of Stokes photons has no preferred direction. This result agrees with Ref. [23], in which Stokes photons are said to be emitted into 4π steradian. In contrast, as the temperature of the cloud is increased, the probability distribution narrows around $\theta = 0$, showing that in the case of warm atomic ensembles, Stokes photons are emitted preferentially along the direction of the pump, as it has been experimentally observed, for instance, in Ref. [22].

The results presented in Fig. (2.2) can be understood in terms of the *which-way* information left in the atoms after emitting a Stokes photon, i.e., the information about the position of the atom that emitted the photon. In the case of cold atomic ensembles, the fact that atoms are fixed would allow us, in principle, to obtain information about the position of the atom that emitted the photon. In this situation, the possible paths of the Stokes photon will not interfere, because which-way information has been left in the ensemble. This can be clearly seen from Eq. (2.16), which for cold atomic clouds takes the form

$$P_{\text{cold}}(\mathbf{k}) = \sum_{i=1}^{N} \left| u\left(\mathbf{r}_{\perp,i}\right) \right|^2 . \tag{2.17}$$

Equation (2.17) shows that emission of Stokes photons from a cold atomic ensemble has no preferred direction. Moreover, notice that it describes a sum of the squared amplitudes of the fields, which is a footprint of an incoherent sum, where interference effects are not present.

In the case of hot atomic ensembles, one can easily show that Eq. (2.8) is a constant within the integration volume, so we can write Eq. (2.16), assuming a large atom number density, as

$$P_{\text{hot}}(\mathbf{k}) = \left| \sum_{i=1}^{N} u\left(\mathbf{r}_{\perp,i}\right) e^{-i\Delta\mathbf{k}\cdot\mathbf{r}_i} \right|^2 . \tag{2.18}$$

We can observe from Eq. (2.18) that interference between possible paths of the Stokes photon is now restored, because which-way information has been erased by the movement of the atoms in the cloud. Interestingly, this which-way information effect has also been observed, for instance, in the context of second-order interference of single photons [38].

It is important to highlight that the results presented here show that whether interference effects are present does not depend on the actual acquisition of information from the system, but on the possibility to obtain such information. This fundamental relationship between interference and indistinguishability has been pointed out, for

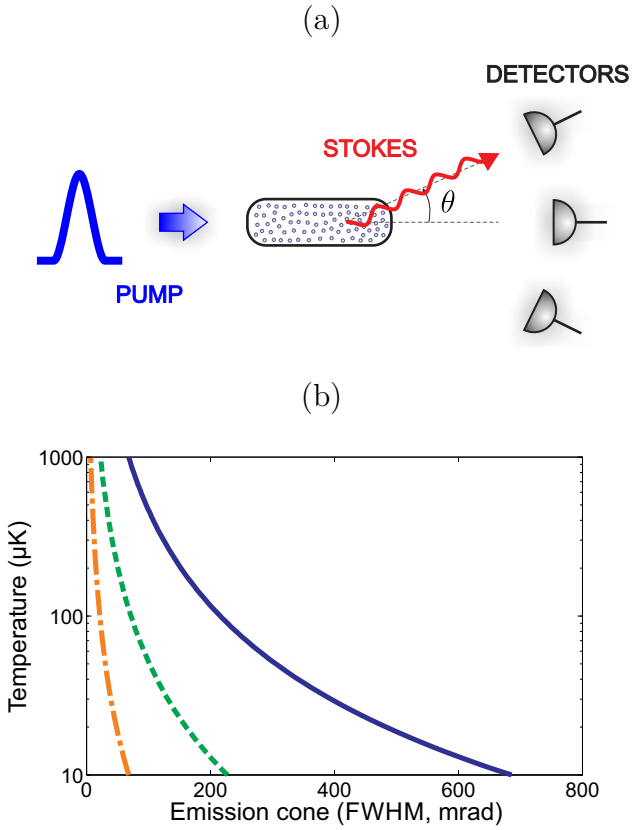

Fig. 2.3 (a) Proposed experimental setup: an array of detectors is used to measure the width of Stokes emission cone in order to determine the temperature of the atomic ensemble. (b) Temperature of the atomic cloud as a function of the full width at half maximum of the emission cone, considering different pulse durations. Solid line: $\tau = 10$ μs; Dashed line: $\tau = 30$ μs; Dash-dotted line: $\tau = 100$ μs.

instance, in Ref. [39].

2.3 Experimental proposal

The close relationship between the width of the Stokes emission cone and the temperature of the atomic ensemble allows us to introduce a new technique for measuring the temperature of atomic clouds. The proposed experimental scheme consists of an array of detectors (or a movable detector) that would be able to detect Stokes photons along different directions, as shown in Fig. 2.3(a). In this way, by measuring the width of the emission cone, we could use Eq. (2.16) to retrieve information about the temperature of the atomic ensemble. To exemplify how the proposed technique would

perform, Fig. 2.3(b) shows the temperature of the atomic ensemble as a function of the full width at half maximum (FWHM) of the emission cone. Notice that, by selecting a sufficiently short pulse, the dependence of the emission cone on the temperature of the ensemble gets smoother. This can be useful for a better discrimination of the width of the emission cone, enhancing thus the precision of the technique. Also, notice that the proposed experimental scheme is not based on the ballistic expansion of the atomic cloud [32], so each measurement can be performed without destroying it.

2.4 Heralded generation of the symmetric atomic state

Another important feature of Eq. (2.9) is that it can also be used to describe how the generation of the symmetric collective atomic state depends on the temperature of the atomic cloud. When a Stokes photon is detected in an arbitrary direction $\mathbf{k}$, i.e., is projected into the state $|\mathbf{k}\rangle$, the corresponding quantum state of the atomic cloud is

$$|\Psi\rangle_a = \sum_{i=1}^{N} S(\mathbf{r}_i, \mathbf{k}) \, |g_1 ... s_i ... g_N\rangle \, . \tag{2.19}$$

The projection of Eq. (2.19) on the symmetric state $|s_a\rangle$ can then be used to find the probability of generating a symmetric state in the atomic ensemble. In the cold atoms case, although Stokes photons are emitted in a larger emission cone, only a small fraction of them (those in a small angle around the pump beam) correspond to the symmetric state [see Figs. 2.4(a,b)]. In contrast, when the temperature of the cloud is increased, which-way information is erased and the emission cone gets narrower [Fig. 2.4(g)]. In this case, as it can be seen from Fig. 2.4(h), photons emitted in all allowed possible directions are in the symmetric state. Notwithstanding, if we want to enhance the flux of detected Stokes photons, we are again forced to detect them in small emission angles around the pump beam. Therefore, in all cases, one needs to detect the Stokes photons in a small cone around the direction of propagation of the pump beam, if the goal is to generate the symmetric collective atomic state. But, as Fig. 2.4 shows, the reason behind this restriction depends on the temperature of the atomic ensemble.

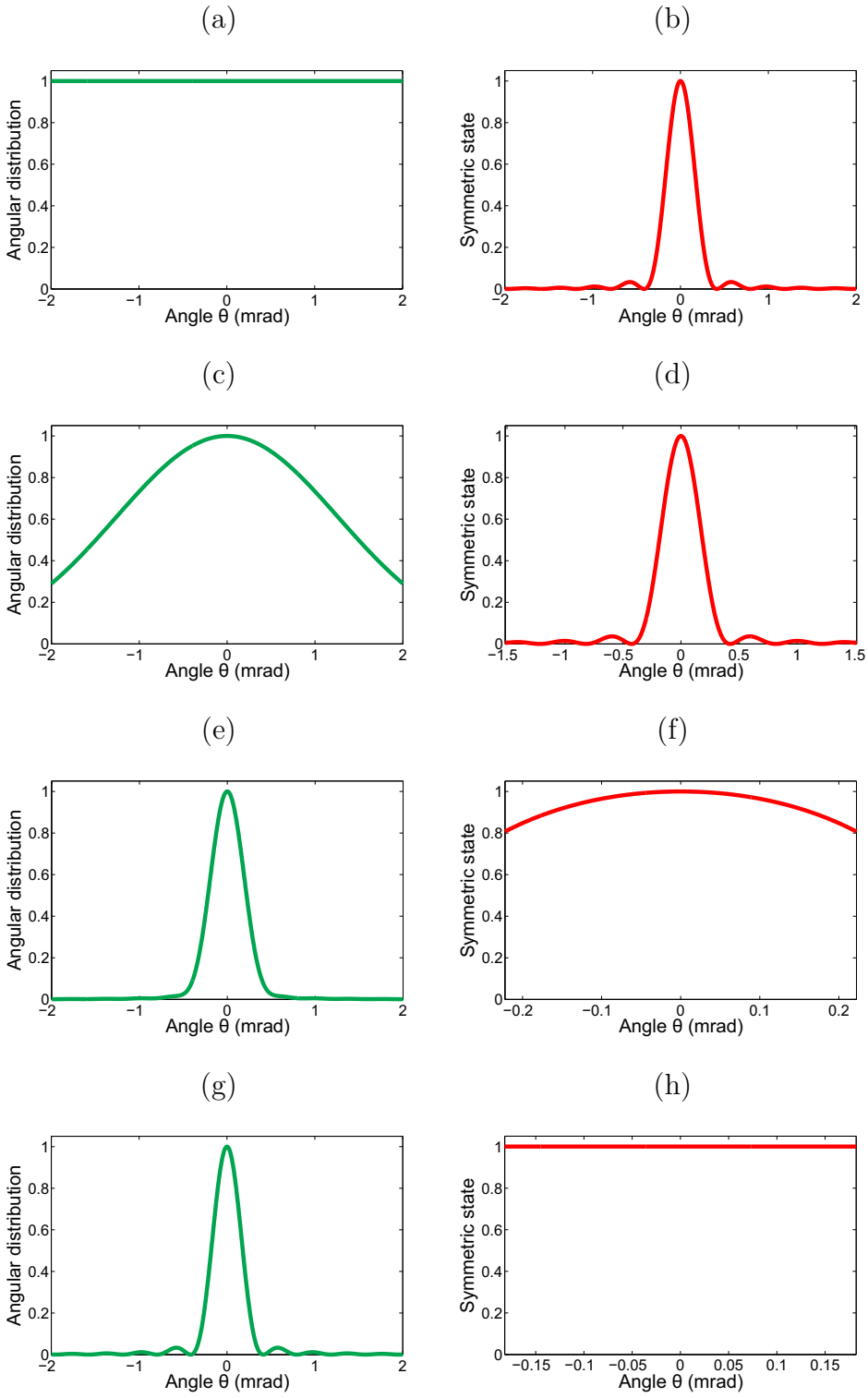

Fig. 2.4 Angular distribution of the emitted Stokes photons [(a),(c),(e) and (g)], and the weight of the symmetric atomic state $|\langle s_a|\Psi\rangle_a|^2$ (within the FWHM of the emission cone) [(b), (d), (f) and (h)] for different radius of the region where atoms are let to move: (a,b) A=1 μm, (c,d) A=100 μm, (e,f) A=1 mm, and (g,h) A=100 mm. Pulse duration: 10 μs.

Conclusions

In this chapter, we have described the relationship that exists between the temperature of an atomic ensemble and the width of the emission cone of spontaneously emitted Stokes photons. Using this fundamental result, we have presented a new nondestructive technique for measuring the temperature of atomic clouds. Furthermore, we have shown that heralded generation of the collective symmetric atomic state requires the detection of the heralding Stokes photon in a narrow cone around the direction of the exciting pulse. For cold atomic clouds, this is the only direction that guarantees the generation of such state, whereas for hot atomic ensembles, it is the direction with the highest efficiency.